

Time resolved imaging of the non-linear bullet mode within an injection-locked spin Hall nano-oscillator

T. M. Spicer,¹ P. S. Keatley,¹ M. Dvornik,² T. H. J. Loughran,¹ A. A. Awad,² P. Dürrenfeld,² A. Houshang,² M. Ranjbar,² J. Åkerman,^{2,3} V. V. Kruglyak,¹ and R. J. Hicken¹

¹*Department of Physics and Astronomy, University of Exeter, EX4 4QL, United Kingdom*

²*Department of Physics, University of Gothenburg, 412 96 Gothenburg, Sweden*

³*Materials Physics, School of ICT, KTH-Royal Institute of Technology, Electrum 229, 164 40 Kista, Sweden*

(Dated: Last updated December 14, 2024)

Time-resolved scanning Kerr microscopy has been used to image large amplitude precessional magnetization dynamics within a spin Hall nano-oscillator (SHNO). The SHNO was formed from a 4 micron diameter Py(5 nm)/Pt(6 nm) mesa defined upon a Al_2O_3 substrate, with triangular Au(150 nm) contacts overlaid. Injection of an RF current was used to phase lock the SHNO to the repetition rate of the laser system. Time resolved imaging revealed that injection of DC current leads to excitation of a non-linear ‘bullet’ mode with a clear threshold behaviour, that can be separated from the small amplitude Ferromagnetic resonance (FMR) induced by the RF current. The out of plane magnetization component is readily detected by means of the polar magneto optical Kerr effect (MOKE). However images obtained by means of longitudinal MOKE measurements are dominated by an artifact arising from the edges of the Au contacts. Micromagnetic simulations suggest that the diameter of the bullet mode is significantly smaller than that of the focused laser spot. Nevertheless, as the DC current is increased above the threshold value, the image of the bullet mode is found to increase in size, suggesting that the bullet becomes increasingly mobile and exhibits significant translational motion relative to the centre of the device. This behaviour may be driven by a reduction of the spin transfer torque at the centre of the device due to heating effects.

INTRODUCTION

The study of spin orbit torques is multi-faceted, with extensive efforts being made to both understand the underlying physical phenomena and realize new applications. The spin torque oscillator (STO) is a nanoscale device in which magnetic auto-oscillations, with frequencies that range from the MHz to GHz regimes, are driven by the spin transfer torque (STT) associated with injection of spin current. The frequency and amplitude of oscillation can be tuned via either an electrical bias current or an applied magnetic field, while the magnetoresistance of the constituent materials leads to the generation of voltage oscillations. Consequently the STO has strong potential for use in magnetic sensing, signal processing, and neuromorphic computing applications [1–3]. High density arrays of STOs can be envisaged that also offer the prospect of mutual synchronisation for increased output power. However it is first necessary to understand the character, localisation and stability of the underlying magnetization dynamics.

While the first STOs exploited spin-polarized current injection, within a spin Hall nano-oscillator (SHNO) the Spin Hall effect (SHE) [4, 5] is used to drive a pure spin current from a heavy metal layer with large spin-orbit interaction into a ferromagnet layer [6–8]. The de-coupling of charge and spin currents opens up new device geometries, enabling the exploitation of magnetic insulators[9], and in the present study, allows for access of an optical probe to the active region of the device.

The generation of magnetic auto-oscillations requires

a critical spin current density to be exceeded. Within the SHNO it is necessary to concentrate the injected charge current within a small region of the heavy metal. This has been achieved by either overlaying thick needle shaped contacts on top of the heavy metal layer [6, 10–14] or by forming a nanoconstriction within the heavy metal/ferromagnet bilayer[15–20]. SHNOs of both kinds have been studied by means of Brillouin Light Spectroscopy (BLS), microwave spectroscopy and micro-magnetic simulations. While the spectral characteristics of the dynamics have been explored, the time-evolution of the magnetization has yet to be measured directly.

In the present work we use time resolved scanning Kerr microscopy (TRSKM)[21, 22] to observe the time dependent magnetization within a SHNO that has been phase locked to an injected microwave current. Formation of the non-linear ‘bullet’ mode is observed when the injected DC current I_{DC} exceeds a threshold value. Comparison with micromagnetic simulations shows that the bullet mode has a diameter small compared to that of the focused optical spot. Nevertheless the apparent diameter of the bullet mode is observed to increase as I_{DC} is increased above the threshold value, suggesting that the bullet has increasing translational motion relative to the centre of the device.

EXPERIMENTAL METHOD

SHNOs were fabricated through a combination of sputter deposition and electron-beam lithography. A $4\mu m$ Py(5 nm)/Pt(6 nm) bi-layer disk was first defined, before

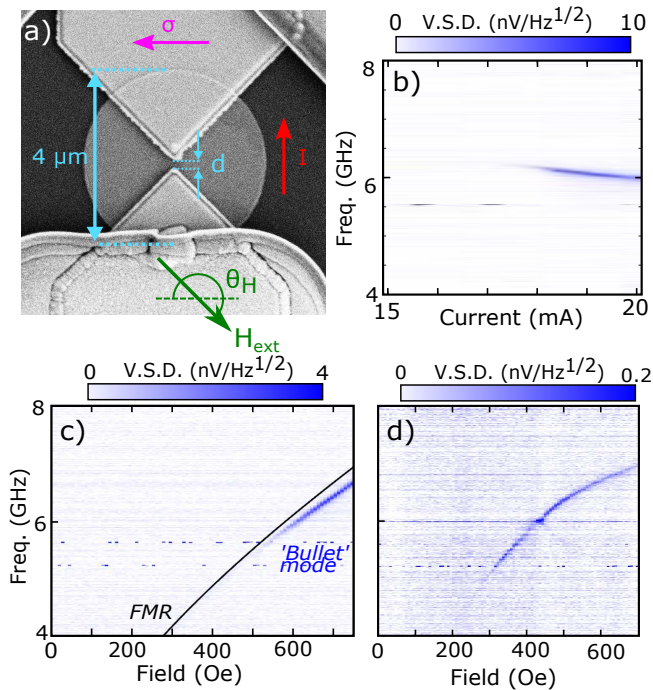


FIG. 1. a) SEM image of a typical SHNO, where I is the injected current, σ the corresponding spin polarization, d the NC separation, and H the magnetic field applied at angle θ_H . b) Voltage Spectral Density (VSD) of microwave emission from a SHNO with $d=240$ nm at fixed magnetic field $H = 650$ Oe and $\theta_H = 210^\circ$ for different values of I_{DC} . c) Emission excited in a SHNO with $d = 240$ nm for $I_{DC} = 18$ mA, with magnetic field H orientated at $\theta_H = 150^\circ$. The solid black line shows the field dependence of the FMR frequency obtained from STT-FMR measurements. d) Emission from the device in (c) when $I_{DC} = 18.5$ mA and I_{RF} has amplitude of 3.5 mA and frequency of 12 GHz.

two triangular Au(150 nm) nanocontacts (NCs), with a tip separation of 200 nm, were overlaid as shown in figure 1a.

The device is designed to concentrate electrical current within the Pt layer at the centre of the disk. Here the charge current is used to generate a spin current, by means of the spin Hall effect, that propagates normal to the plane of the device into the Py layer. Once the STT compensates the damping, a self-localized non-linear mode is formed, that has been described as a spin wave bullet. While other modes can be supported within the disk ([14] demonstrates propagating waves when the Py is magnetized normal to the plane of the device), the bullet mode is of particular interest due to its narrow linewidth and the tuneability of its frequency.

Initial characterization was carried out by means of microwave frequency electrical measurements, that exploit the magnetoresistive response of the Py layer. A single high frequency ground-signal-ground electrical probe was used to make electrical contact to a selected device and connect it to a bias-tee. DC current I_{DC} and RF current

I_{RF} were then supplied through the inductive and capacitive arms respectively, while the RF signal returned from the device was directed into a spectrum analyzer via a circulator and +24 dB pre-amplifier. TRSKM measurements were performed with a vector-quadrant bridge detector that exploits different Kerr effect geometries in order to simultaneously detect the three spatial components of the dynamic magnetization and the optical reflectance [23]. For the magnetization dynamics to be observed in a stroboscopic fashion, the dynamics must be synchronised with the laser pulses via the injected I_{RF} that has frequency equal to a direct multiple of the 80 MHz laser repetition rate. The phase of I_{RF} can then be adjusted relative to the laser's master clock so that the evolution of the magnetization dynamics through the cycle of the RF signal can be observed. Measurements were performed with phase modulation of I_{RF} to enhance the signal to noise ratio. The laser pulses had centre wavelength of 800 nm, and were focused to a spot of ~ 870 nm FWHM diameter by a microscope objective with working distance of 10.1 mm and 0.55 numerical aperture [24].

ELECTRICAL MEASUREMENTS

Microwave frequency electrical measurements were performed to identify the spin wave bullet and confirm its locking to I_{RF} . Figure 1b shows the microwave emission from a SHNO for a fixed field and increasing I_{DC} . The onset of emission is observed to occur at $I_{DC} \sim 18$ mA, whereupon the frequency red-shifts with increasing I_{DC} and is still present at $I_{DC} = 20$ mA. No emission is observed if the sign of either the applied field H or I_{DC} is changed, in agreement with the expected symmetry of the spin Hall effect. Figure 1c shows the field and frequency dependence of both the Ferromagnetic Resonance (FMR), determined from separate STT-FMR measurements (consistent with previous work [11, 25]), and the microwave emission. For a fixed frequency, microwave emission is observed at a field close to but greater than that of the FMR mode. The dependence of the frequency of emission upon H and I_{DC} is consistent with previous observations of the spin wave bullet [13].

Before stroboscopic TRSKM measurements can be attempted, it is necessary to demonstrate that the bullet mode can be synchronised to I_{RF} . Figure 1d clearly demonstrates that a bullet mode with frequency of 6 GHz can be locked to an I_{RF} of 12 GHz frequency. As the strength of the applied field is varied, the frequency of the microwave emission approaches 6 GHz and is 'pulled' towards the locking regime. Within this region an increase in output power and reduction in linewidth is observed. Outside of this regime an intermodulation mode can be observed, decreasing in frequency with increasing field. A large I_{RF} of ~ 3.5 mA amplitude was required to achieve even a narrow locking range, which may be attributed to

the effect of thermal noise enhanced by the spin current [10].

TRSKM OBSERVATIONS

A previous optically-detected STT-FMR study of similar devices [26] revealed a reduction of the STT at the centre of the device that was attributed to local heating effects. Therefore TRSKM measurements were performed with the frequency of I_{RF} set to 6 GHz so as to minimise the amplitude of I_{RF} required to achieve locking [27].

Figure 2a shows TRSKM images acquired firstly with the bullet mode locked to I_{RF} , and secondly when I_{RF} is still present but $I_{DC} = 0$ mA. In the latter case, I_{RF} drives a finite-amplitude off-resonance FMR since the locking field overlaps the finite width FMR line profile at this frequency. The addition of I_{DC} leads to additional dynamics in all three magnetic channels. In the polar magnetization channel, localized precession is observed between the NC tips, with a different phase to the dynamics in the extended disk (additional data [27]). By subtracting the images acquired with and without I_{DC} , the dynamic magnetization response due to I_{DC} may be estimated (lower part of figure 2a). The subtracted images for the two in-plane (horizontal and vertical) channels each exhibit a spatially antisymmetric structure centred on the peak observed in the polar contrast, but occupying a somewhat larger area of $\sim 2\mu\text{m}$ diameter. The subtraction yields negligible residual contrast in the extended region of the disk, confirming that the bullet mode is tightly confined at the centre of the disk.

Further measurements performed at different time delays [27] confirmed that the contrast in the three magnetic channels oscillates with the same period as that of I_{RF} . However the contrast in the three channels was observed to oscillate with the same relative phase, which is not expected if the magnetization undergoes a circular or elliptical precession. Furthermore, since the magnetic field is applied 30° from the horizontal axis, the amplitude of the dynamic magnetization detected in the TRSKM experiment is expected to be significantly greater in the vertical direction as compared to the horizontal direction, while in fact these two components were found to have comparable amplitude within the experiment. Therefore, to aid the interpretation of the experimental data, micromagnetic simulations were performed, using the MuMax 3 package after the current distribution and associated Oersted field had been calculated in COMSOL [27–29].

Images of the simulated bullet mode are presented in figures 3a for the magnetic field configuration of figure 2. Initial simulations showed that the bullet mode quickly escapes the active area and is damped within the extended disk. In order to sustain the mode a pinning site

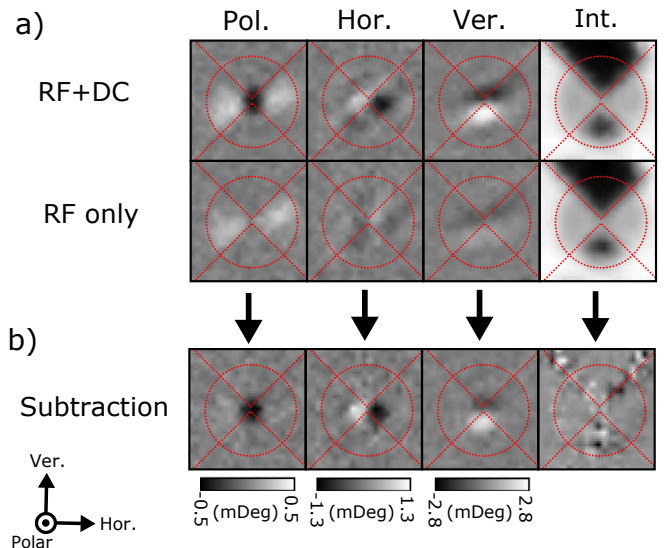


FIG. 2. a) TRSKM images acquired from the polar (out of plane), horizontal, vertical and reflected intensity channels of the vector bridge detector for a SHNO with $d = 200$ nm, with $H = 650$ Oe, $\theta_H = 210^\circ$, and $I_{RF} = 1.4$ mA at a frequency of 6 GHz. $I_{DC} = 16$ mA and 0 mA in the upper and lower panels respectively. (b) The difference of the upper and lower images from (a) is shown, revealing contrast due to the presence of I_{DC} only. Each image shows a $5\mu\text{m}$ square region.

was found to be necessary, which could take the form of either a single cell discontinuity of the magnetization, or in the case of 3a, a localized 5% reduction in saturation magnetization with Gaussian spatial profile of ~ 240 nm FWHM. Such simulations successfully yielded a bullet mode that was stable for a finite range of I_{DC} values, as well as an additional mode that was localized in the non-uniform magnetic field landscape generated by the Oersted field associated with the injected charge current. The latter mode lies at higher frequency than the bullet mode. Since it was not observed in room temperature spectroscopy measurements shown in figure 1, it is not expected to appear in TRSKM measurements. Both the bullet and field-localized modes were found to have spatial and spectral character consistent with previous simulations [13, 14].

While the the bullet mode exhibits large angle precession, the snapshots in figure 3a give no indication of the spatially antisymmetric character observed in the experimentally measured horizontal and vertical components. To better understand the simulated dynamics, two regions can be defined, (i) the core of the bullet mode which undergoes the largest angle of precession, and (ii) the dynamic magnetization in the extended disk. Figure 3b demonstrates that the magnetization in region (ii) undergoes elliptical precession about an axis parallel to the applied field, increasing drastically in amplitude for points closer to the core in region (i). On the border between the two regions at $x = -35$ nm, the average

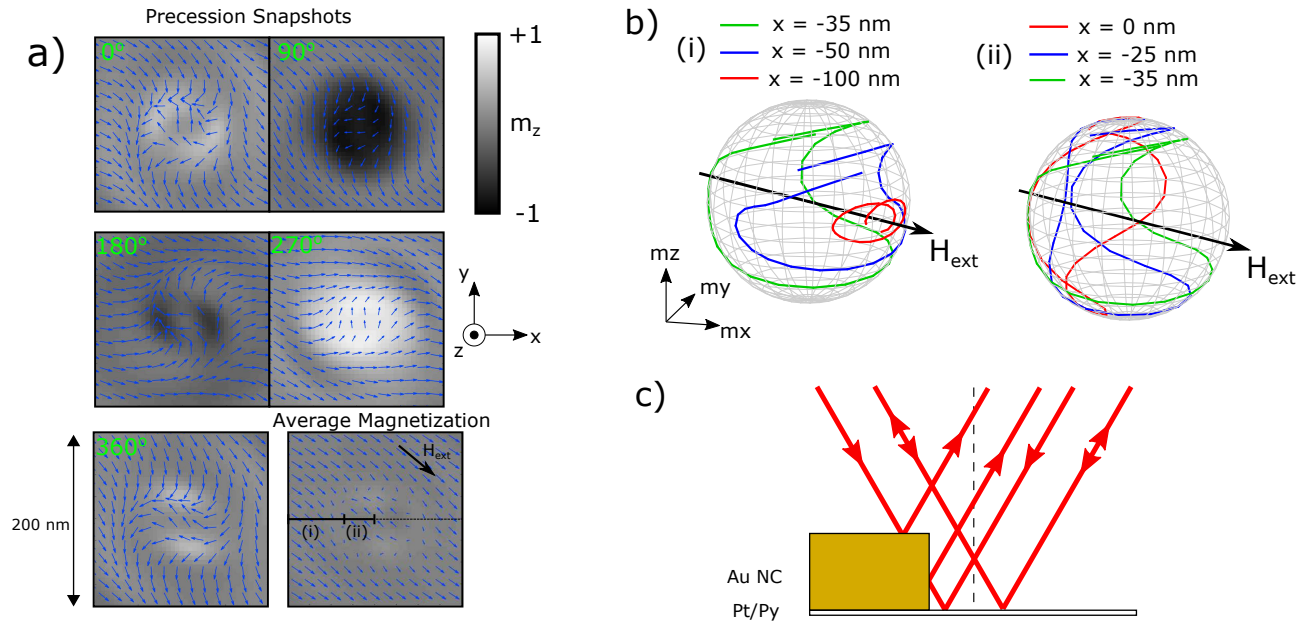


FIG. 3. a) Snapshots of the stable precession observed in micromagnetic simulations at different values of phase within the cycle of auto-oscillation. The arrows indicate the projection of the magnetization within the plane, while the grayscale represents the out of plane magnetization component. The coordinate axes are shown with the origin assumed to be at the centre of the device. The image of the time averaged magnetization indicates two regions associated with (i) the bullet mode with ~ 70 nm diameter, and (ii) the surrounding region. b) Trajectories of the magnetization for points on the x axis within both regions (i) and (ii), over 1 cycle of oscillation at the fundamental frequency. c) Schematic to show the origin of the optical artefact that generates contrast in the horizontal and vertical channels. Arrows indicate the direction of propagation of rays, while dashed lines indicate those obstructed by the NCs.

magnetization is close to zero with an in-plane precession angle of $\sim 270^\circ$. Within the core the precession amplitude increases further such that the magnetization trajectory crosses over itself, so that here the magnetization can be said to precess about a direction anti-parallel to the applied field. The magnetization precesses with the same phase at all positions within the disk, i.e. the maximum amplitude of the out of plane magnetization component was observed at all positions at the same point in time, and so TRSKM images of the in-plane magnetization components are also expected to be spatially uniform (further details in [27]). Simulations performed with an additional I_{RF} demonstrated slightly improved stability of the bullet, but otherwise showed dynamics of similar character.

Difference images, calculated from images separated by 180° in phase, were convolved with a Gaussian profile of 870 nm FWHM width to more closely reproduce the experimental images. However it again proved impossible to reproduce the spatially antisymmetric contrast observed experimentally in the vertical and horizontal channels. Further experimental tests showed that the antisymmetric contrast was observed only when the bullet mode was present, ruling out mechanisms such as polarization of the Pt by I_{RF} via the spin Hall effect. Therefore it was concluded that the in-plane contrast must be an artefact associated with the optical probe passing

over the edge of the 150 nm thick NCs, while in proximity to the bullet mode. Figure 3c provides a schematic representation of the likely mechanism. As the probe passes over the NCs the beam returning to the detector is partially obstructed. Crucially the symmetry between rays propagating in opposite directions within the cone is broken. The resulting difference in intensity of the two halves of the back-reflected beam, combined with a finite polar Kerr rotation due to the bullet mode, manifests as a signal similar to that due to the longitudinal magneto optical Kerr effect for a sample with in-plane magnetization[30]. It follows from the NC geometry that a top-bottom antisymmetry is observed in the vertical channel and a left-right antisymmetry in the horizontal channel.

The polar images are unaffected by the artefact although it is necessary to bear in mind the effect of the finite optical spot size when making comparison with the simulations. Figure 4a shows polar images acquired for different I_{DC} values, with the phase of I_{RF} fixed. The maximum absolute Kerr rotation was extracted from the images and plotted in figure 4b, while in figure 4c the images from 4a have been replotted after subtraction of the image for which $I_{DC} = 0$. For small I_{DC} values the amplitude of the FMR mode increases gradually with increasing I_{DC} as the injection of DC spin current into the Py layer acts to compensate the damping. For $I_{DC} \geq 10$

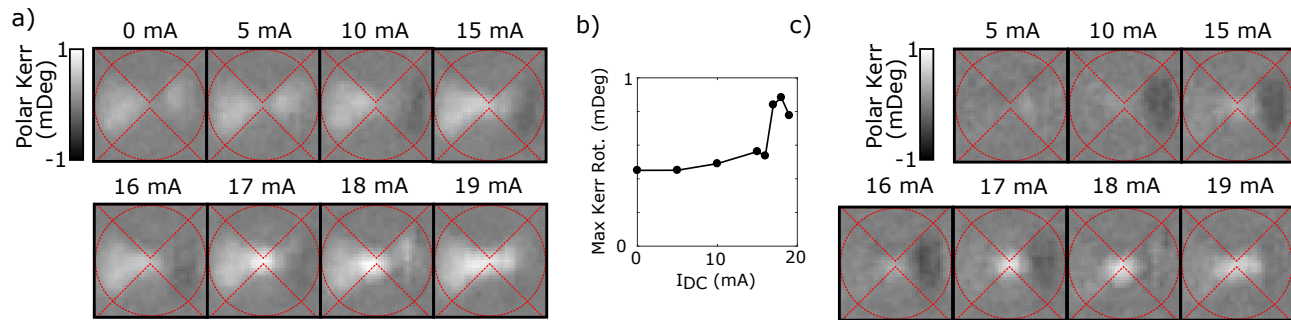


FIG. 4. a) Polar TRSKM images acquired for different I_{DC} values with the phase of I_{RF} fixed. b) Maximum absolute values of polar Kerr rotation extracted from the images in (a). (c) TRSKM images from (a) after subtraction of the $I_{DC} = 0$ mA image. All images were recorded from a SHNO with $d = 240$ nm, with $I_{RF} = 0.8$ mA, $H = 650$ Oe and $\theta_H = 210^\circ$.

mA a region of negative contrast appears to the right of the NCs. In fact as I_{DC} is increased the contrast outside the central region of the disk becomes more spatially antisymmetric about the the centre line. This is consistent with the FMR increasingly being driven by the out of plane component of the Oersted field as heating associated with I_{DC} suppresses the STT which instead favours a spatially symmetric response [26].

The microwave spectroscopy data of figure 1b previously revealed the presence of a bullet mode for $I_{DC} = 18 \rightarrow 20$ mA. However figure 4 shows strong out of plane dynamics localized at the NC tips for $I_{DC} = 17$ mA, that is still present when $I_{DC} = 19$ mA. The reduction of the threshold value for I_{DC} is due to the presence of finite I_{RF} , as observed previously [10]. Figures 4a and c also demonstrate that the extent of localization of the bullet mode depends upon I_{DC} . Comparing the images for $I_{DC} = 17 \rightarrow 19$ mA, the bullet mode is observed to occupy a larger region as I_{DC} is increased, with some reduction in the maximum Kerr amplitude. Since the diameter of this region is large compared to that of the bullet mode in figure 3a, this suggests that the bullet exhibits translational motion relative to the center of the disk even though the precession remains phase-locked to I_{RF} .

Previously, an optically-detected STT-FMR study of similar devices revealed local minima, in both the in-plane Oersted field and the STT, at the centre of the disk, presumably due to heating associated with the injected current. The bullet mode may therefore move away from the centre to the neighbouring region where the STT is larger, and may then either oscillate or gyrate about the centre. The bullet could either establish a stable trajectory, or alternatively escape and be damped in the extended disk, as observed in simulations in the absence of a pinning site [27], allowing another bullet to form in the centre and repeat the process. Increasing I_{DC} is likely to broaden the minimum in the STT at the centre of the disk, pushing the bullet further from the centre. Given that the linewidth of the microwave emission in 1b

is only weakly dependent on I_{DC} , formation of a stable trajectory is the more likely scenario.

In summary, time resolved images of the non-linear bullet mode within a SHNO have been obtained. The bullet was successfully injection-locked to a microwave current, enabling stroboscopic TRSKM measurements to be performed. The microwave current simultaneously excites an FMR mode, but a simple subtraction procedure allows the contrast associated with the bullet to be isolated. While the out of plane component of the precessing magnetization within the bullet was unambiguously observed, measurements of the in-plane components were obscured by an artefact resulting from the edges of the thick electrical contacts. The localization of the bullet near the centre of the disk was found to decrease as the injected DC current was increased above the threshold value. Localized heating has been shown to modify the spatial distribution of charge current and STT within the device. Further work is now required to determine the trajectory of the bullet within this landscape.

We acknowledge financial support from the Engineering and Physical Sciences Research Council (EPSRC) of the United Kingdom, via the EPSRC Centre for Doctoral Training in Metamaterials (Grant No. EP/L015331/1) and EPSRC grants EP/I038470/1 and EP/P008550/1.

-
- [1] M. D. Stiles and J. Miltat, *Topics in Applied Physics* **101**, 225 (2006).
 - [2] T. Jungwirth, J. Wunderlich, and K. Olejník, *Nature Materials* **11**, 382 (2012), arXiv:1411.3249v1.
 - [3] A. V. Chumak, V. I. Vasyuchka, A. A. Serga, and B. Hillebrands, *Nature Physics* **11**, 453 (2015).
 - [4] Y. K. Kato, R. C. Myers, a. C. Gossard, and D. D. Awschalom, *Science* **306**, 1910 (2004).
 - [5] A. Hoffmann, *IEEE Transactions on Magnetics* **49**, 5172 (2013).
 - [6] V. E. Demidov, S. Urazhdin, H. Ulrichs, V. Tiberkevich, A. Slavin, D. Baither, G. Schmitz, and S. O. Demokritov, *Nature Materials* **11**, 1028 (2012).
 - [7] A. Brataas, A. D. Kent, and H. Ohno,

- Nature Materials **11**, 372 (2012).
- [8] R. Dumas, S. Sani, S. Mohseni, E. Iacocca, Y. Pogoryelov, P. Muduli, S. Chung, P. Durrenfeld, and J. Åkerman, IEEE Transactions on Magnetics **50**, 1 (2014).
- [9] A. Hamadeh, O. d’Allivy Kelly, C. Hahn, H. Meley, R. Bernard, A. H. Molpeceres, V. V. Naleto, M. Viret, A. Anane, V. Cros, S. O. Demokritov, J. L. Prieto, M. Muñoz, G. de Loubens, and O. Klein, Physical Review Letters **113**, 197203 (2014), arXiv:1405.7415.
- [10] V. E. Demidov, H. Ulrichs, S. V. Gurevich, S. O. Demokritov, V. S. Tiberkevich, a. N. Slavin, A. Zholud, and S. Urazhdin, Nature communications **5**, 3179 (2014).
- [11] R. H. Liu, W. L. Lim, and S. Urazhdin, Physical Review Letters **110**, 147601 (2013).
- [12] M. Ranjbar, P. Durrenfeld, M. Haidar, E. Iacocca, M. Balinskiy, T. Q. Le, M. Fazlali, A. Houshang, A. A. Awad, R. K. Dumas, and J. Åkerman, IEEE Magnetics Letters **5**, 1 (2014).
- [13] H. Ulrichs, V. E. Demidov, and S. O. Demokritov, Applied Physics Letters **104**, 042407 (2014).
- [14] A. Giordano, M. Carpentieri, A. Laudani, G. Gubbiotti, B. Azzerboni, and G. Finocchio, Applied Physics Letters **105**, 042412 (2014), arXiv:1407.7655.
- [15] V. E. Demidov, S. Urazhdin, A. Zholud, A. V. Sadovnikov, and S. O. Demokritov, Applied Physics Letters **105**, 172410 (2014).
- [16] A. A. Awad, P. Dürrenfeld, A. Houshang, M. Dvornik, E. Iacocca, R. K. Dumas, and J. Åkerman, Nature Physics **13**, 292 (2016).
- [17] T. Kendziorczyk and T. Kuhn, Physical Review B - Condensed Matter and Materials Physics **93**, 1 (2016).
- [18] H. Mazraati, S. Chung, A. Houshang, M. Dvornik, L. Piazza, F. Qejvanaj, S. Jiang, T. Q. Le, J. Weissenrieder, and J. Åkerman, Applied Physics Letters **109**, 242402 (2016).
- [19] M. Zahedinejad, A. A. Awad, P. Durrenfeld, A. Houshang, Y. Yin, P. K. Muduli, and J. Åkerman, IEEE Magnetics Letters **8**, 1 (2017).
- [20] B. Divinskiy, V. E. Demidov, A. Kozhanov, A. B. Rinkevich, S. O. Demokritov, and S. Urazhdin, Applied Physics Letters **111** (2017), 10.1063/1.4993910.
- [21] P. Gangmei, P. S. Keatley, W. Yu, R. J. Hicken, M. a. Gubbins, P. J. Czoschke, and R. Lopusnik, Applied Physics Letters **99**, 2009 (2011).
- [22] R. A. J. Valkass, T. M. Spicer, E. Burgos Parra, R. J. Hicken, M. A. Bashir, M. A. Gubbins, P. J. Czoschke, and R. Lopusnik, Journal of Applied Physics **119**, 233903 (2016).
- [23] R. A. J. Valkass, T. M. Spicer, E. Burgos Parra, R. J. Hicken, M. A. Bashir, M. A. Gubbins, P. J. Czoschke, and R. Lopusnik, Journal of Applied Physics **119** (2016), 10.1063/1.4954018.
- [24] P. S. Keatley, S. R. Sani, G. Hrkac, S. M. Mohseni, P. Dürrenfeld, J. Åkerman, and R. J. Hicken, Journal of Physics D: Applied Physics **50**, 164003 (2017).
- [25] L. Liu, T. Moriyama, D. C. Ralph, and R. A. Buhrman, Physical Review Letters **106**, 036601 (2011).
- [26] As yet unpublished work under the title ‘Spatial Mapping of Torques within a Spin Hall Nano-oscillator’, TRSKM measurements on FMR.
- [27] See Supplemental Material at [URL tbc] containing additional injection locking data, and micro-magnetic results.
- [28] *Comsol 5.2a user manual*.
- [29] A. Vansteenkiste, J. Leliaert, M. Dvornik, M. Helsen, F. Garcia-Sanchez, and B. Van Waeyenberge, AIP Advances **4**, 107133 (2014), arXiv:1406.7635.
- [30] P. S. Keatley, V. V. Kruglyak, R. J. Hicken, J. R. Childress, and J. A. Katine, Journal of Magnetism and Magnetic Materials **306**, 298 (2006).